Electronic Supplementary Information

Low-temperature molten salt synthesis of MoS_2@CoS_2 heterostructures for efficient hydrogen evolution reaction

Song He,[a] Hongfang Du,*[a] Ke Wang,[a] Qianchi Liu,[a] Jinmeng Sun,[a] Yuhang Liu,[a] Zhuzhu Du,[a] Linghai Xie,[a,c] Wei Ai,*[a] and Wei Huang*[a,b,c]

[a]*Institute of Flexible Electronics (IFE), Northwestern Polytechnical University (NPU), 127 West Youyi Road, Xi'an 710072, China*

[b]*Key Laboratory of Flexible Electronics (KLOFE) & Institute of Advanced Materials (IAM), Jiangsu National Synergetic Innovation Center for Advanced Materials (SICAM), Nanjing Tech University (NanjingTech), 30 South Puzhu Road, Nanjing 211816, China*

[c]*Key Laboratory for Organic Electronics & Information Displays (KLOEID) and Institute of Advanced Materials (IAM), SICAM, Nanjing University of Posts & Telecommunications, Nanjing 210023, Jiangsu, China*

*Correspondence authors. Email: iamhfdu@nwpu.edu.cn, iamwai@nwpu.edu.cn, iamwhuang@nwpu.edu.cn

1 Experimental Section

1.1 Chemicals

Cobalt nitrate hexahydrate ($Co(NO_3)_2 \cdot 6H_2O$, 99%, Adamas-beta), ammonium molybdate ($(NH_4)_6Mo_7O_{24} \cdot 4H_2O$, 99%, Adamas-beta), potassium thiocyanate (KSCN, 97.18%, Hushi) were bought from Tansoole. Nafion (5 wt.% in lower aliphatic alcohols and water mixture) was purchased from Sigma-Aldrich. All chemicals were used as received without further purification.

1.2 Synthesis of $MoS_2@CoS_2$, MoS_2, and CoS_2

For the synthesis of $MoS_2@CoS_2$ heterostructures, 0.1 g $(NH_4)_6Mo_7O_{24} \cdot 4H_2O$, 0.8 g $Co(NO_3)_2 \cdot 6H_2O$, and 20 g KSCN were mixed together, the molar ratio of Mo to Co was about 0.2. Next, the mixture was loaded to a beaker and heated to 300 °C in a muffle furnace for 2 h. A black and dense solid solution was obtained at the end of the reaction. The product was collected by dissolving the excessive KSCN with DI water, and washed with DI water and ethanol for several times. Finally, the $MoS_2@CoS_2$ powder was dried in a vacuum oven at 80 °C for 12 h. MoS_2 and CoS_2 were also synthesized under similar experimental procedures with $(NH_4)_6Mo_7O_{24} \cdot 4H_2O$ and $Co(NO_3)_2 \cdot 6H_2O$ as the precursor, respectively.

1.3 Synthesis of FeS_2, NiS_2, and SnS_2

For the synthesis of FeS_2, NiS_2 and SnS_2, an equimolar amount of $Fe(NO_3)_2 \cdot 9H_2O$, $NiSO_4$, and $SnCl_2$ was used as the transition metal precursors, respectively. While the detail experimental procedures were similar to the preparation of $MoS_2@CoS_2$.

1.4 Characterizations

X-ray diffraction (XRD) data were recorded on an X-ray diffractometer (Bruker D8 ADVANCE) with Cu Ka radiation (λ= 1.5406 Å). Scanning electron microscopy (SEM) and EDS measurements were carried out with a scanning electron microscope (FEI Verios G4). Transmission electron microscopy (TEM) analysis was performed on a transmission electron microscope (FEI Talos F200X TEM). X-ray photoelectron spectroscopy (XPS) data were recorded with a Thermo Escalab 250Xi instrument (Thermo Fisher).

1.5 Electrochemical measurements

All electrochemical measurements were conducted with a CHI 760E potentiostat in a conventional three electrode setup, in which a graphite rod was served as counter electrode, a saturated calomel electrode (SCE) equipped with a salt bridge was applied as reference electrode, a glass carbon electrode (GCE, Φ = 4.0 mm) was used as working electrode, and 0.5 M H_2SO_4 solution was used as electrolyte. For the preparation of catalyst ink, 10.0 mg catalyst and 2.0 mg carbon black were dispersed in 500 μL ethanol containing 25 μL Nafion (5 wt%), followed by treating in an ultrasonic bath for 15 minutes to get a homogeneous mixture. After then, 6.28 μL of the ink was transferred to a newly polished GCE and dried at room temperature. The loading of the active material was determined to be 1.0 mg cm^{-2}. Linear sweep voltammetry (LSV) curves were recorded at a scan rate of 5.0 mV s^{-1}. The electrochemical impedance spectroscopy (EIS) tests were conducted in a frequency range of 0.1-100K Hz with an AC amplitude of 5.0 mV under a static HER overpotential of 200 mV.

Stability probed via cyclic voltammetry (CV) cycles was conducted in a potential range of -0.15 ~ 0.1 V at a scan rate of 100 mV s^{-1}. All the potentials were converted to the reversible hydrogen electrode (RHE) via the Nernst equation: $E_{RHE} = E_{SCE} + 0.242 + 0.059pH$ (V).[1, 2] All the electrochemical data were *i*R corrected according to the series resistance measured in EIS measurements.[3]

1.6 Theoretical calculations

All static calculations were carried out using spin-polarized density functional theory (DFT) with generalized gradient approximation (GGA) of Perdew-Burke-Ernzerhof (PBE) as implemented in VASP 5.4.4 code.[4, 5] The cutoff energy of plane-wave basis set was 400 eV and single gamma-point grid sampling was used for Brillouin zone integration. Atomic positions and cell parameters were optimized by conjugate gradient algorithm until the forces were less than 0.01 eV/Å. The hydrogen adsorption free energies were determined in the same way as in previous studies, which was estimated to be about 0.24 eV for ZPE, entropy and enthalpy correction.[6] The horizontal lattice parameters of single layer MoS_2 was optimized with 5 Mo atoms × 6 Mo atoms in size (ICSD-84180).[7] CoS_2(001)-p(3×3) slab model was adopted to model CoS_2 substrate with bottom S-Co-S layer was fixed. The lattice parameters of CoS_2 and heterojunction were kept as reported experimental results (ICSD-86351).[8] Periodic boundary conditions were used in all directions and at least 12 Å of vacuum was used in the z-direction to separate the slabs.

2 Supporting figures

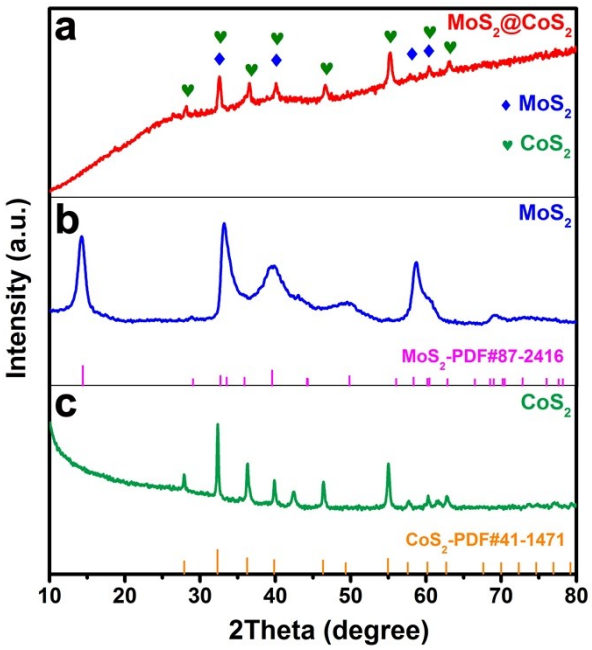

Fig. S1 XRD patterns of (a) MoS_2@CoS_2, (b) MoS_2, and (c) CoS_2.

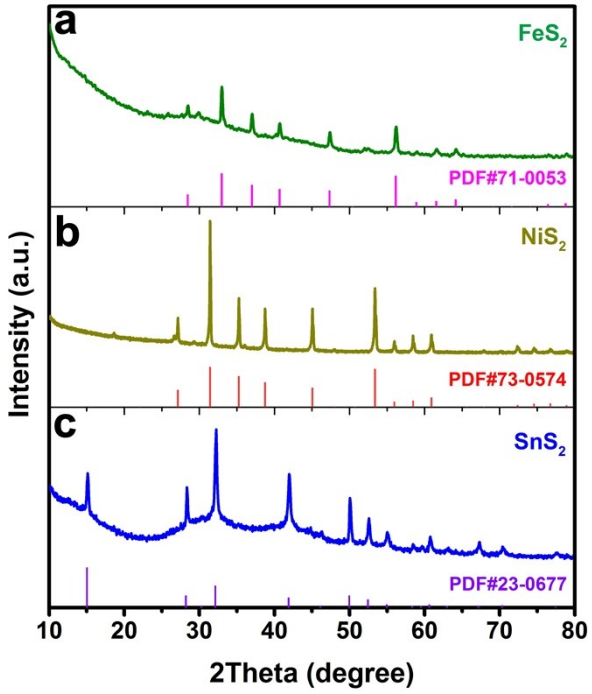

Fig. S2 XRD patterns of (a) FeS_2, (b) NiS_2, and (c) SnS_2.

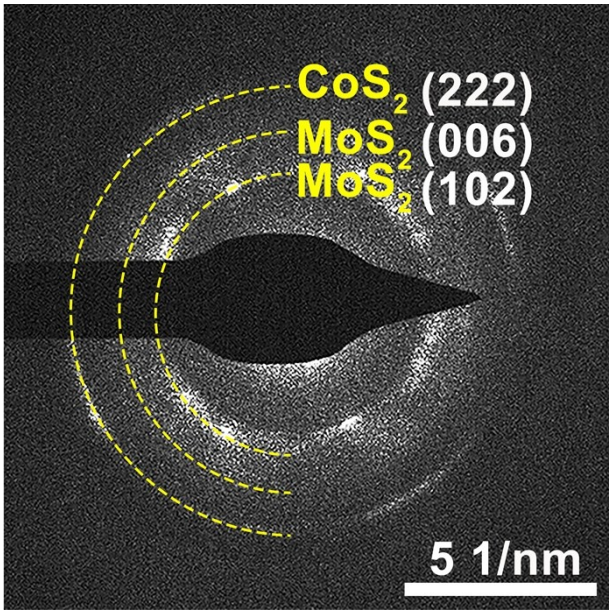

Fig. S3 SAED pattern of MoS_2@CoS_2.

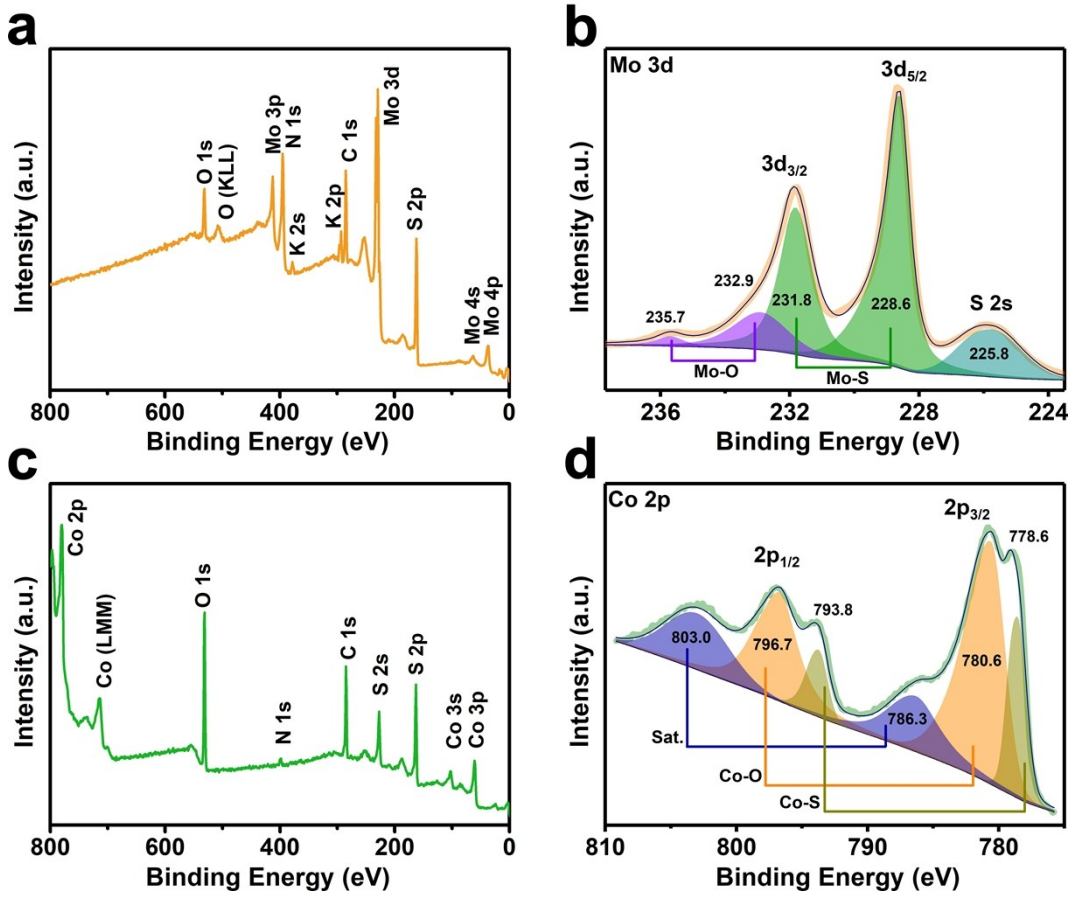

Fig. S4 (a) XPS survey and (b) Mo 3d spectra of MoS_2; (c) XPS survey and (d) Co 2p spectra of CoS_2.

Table S1 Chemical composition of MoS_2@CoS_2, MoS_2 and CoS_2 based on XPS results.

Contents / Catalysts	S (Wt. %)	Mo (Wt. %)	Co (Wt. %)	S (At. %)	Mo (At. %)	Co (At. %)	$Mo_{(At.\ \%)}/Co_{(At.\ \%)}$
MoS_2@CoS_2	47.72	24.93	27.35	67.32	11.73	20.95	0.6
MoS_2	38.31	61.69		65.06	34.94		
CoS_2	53.30		46.70	67.76		32.24	

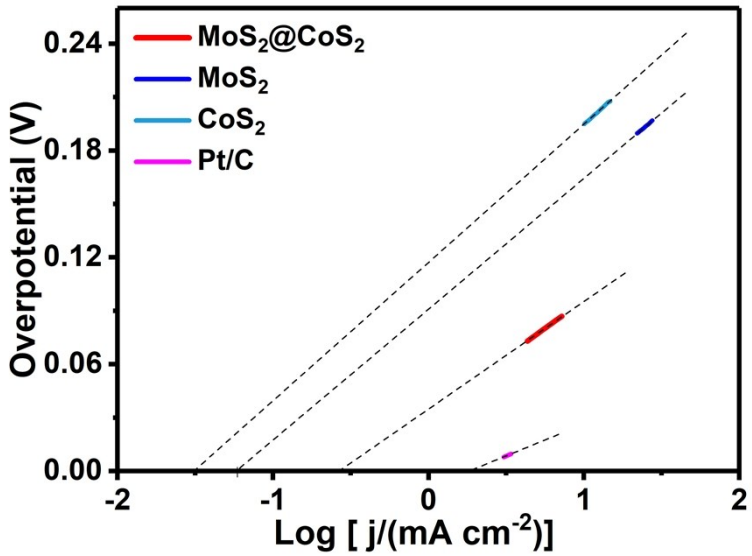

Fig. S5 Estimation of exchange current densities.

The exchange current density (i_0) is calculated via the extrapolation of corresponding Tafel plot. When the overpotential is 0, as revealed in Fig. S5, the log(j) values for MoS_2@CoS_2, MoS_2, CoS_2, and Pt/C are determined to be -0.55, -1.22, -1.5, and 0.28, respectively. Accordingly, the i_0 is calculated to be 0.28 mA cm^{-2} for MoS_2@CoS_2, 6.08×10^{-2} mA cm^{-2} for MoS_2, 3.16×10^{-2} mA cm^{-2} for CoS_2, and 1.91 mA cm^{-2} for Pt/C.

Table S2 Catalytic performance comparison of MoS_2@CoS_2 with the recently reported MoS_2- and CoS_2-based HER catalysts.

Catalysts	η_{10}	Tafel (mV dec^{-1})	Reference
$Co_9S_8/MoS_2/Ni_3S_2$-NF	103	55	*J. Am. Chem. Soc.*, 2019, **141**, 10417.
MoS-CoS	134	60	*Adv. Sci.*, 2019, **6**, 1900140.
MoS_2/CoS_2 NT	90	30	*J. Mater. Chem. A*, 2019, **7**, 13339
CoS_2-C@MoS_2	173	61	*ACS Sustainable Chem. Eng.*, 2019, **7**, 2899.
S-MoS_2@C	136	78	*Adv. Energy Mater.*, 2019, **9**, 1802553.
Co_9S_8@MoS_2	171	123	*ACS Appl. Mater. Interfaces*, 2018, **10**, 1678.
CoS_x@MoS_2	239	103	*ACS Sustainable Chem. Eng.*, 2018, **6**, 12961
MoS_2@NSCS	158	82	*Appl. Catal., B*, 2020, **263**, 118352.
NPC@MoS_2	178	58	*Catal. Today*, 2019, **330**, 259.
$MoS_2/CoNi_2S_4$	81	67	*Adv. Funct. Mater.*, 2019, 1908520.
0.75-Sv-MoS_2	194	78	*Angew. Chem.*, 2019, **131**, 2051.
EA-2H/1T/rGO	186	49	*Small*, 2019, **15**, 1804903.
N-MoS_2/CN	114	46.8	*J. Am. Chem. Soc.*, 2019, **141**, 18578.
Ag_2S/MoS_2/rGO	190	56	*ACS Appl. Mater. Interfaces*, 2019, **11**, 22380.
1D-DRHA MoS_2	119	50.7	*Appl. Catal., B*, 2019, **258**, 117964.
Hexagonal MoS_2 flakes	105	53	*J. Mater. Chem. A*, 2019, **7**, 27603.
MoS_2 nanoscroll	153	73	*ACS Energy Lett.*, 2019, **4**, 2830.
V-doped MoS_2	194	59	*Appl. Catal., B*, 2019, **254**, 432.
3D-Co-MoS_2/G	143	71	*Nano Energy*, 2019, **61**, 611.
1T-MoS_2/CC	151	55	*Appl. Catal., B*, 2019, **246**, 296.
Fractal-shaped MoS_2	185	45	*Nano Energy*, 2018, **51**, 786.
MoS_2 ML	126	72	*Adv. Energy Mater.*, 2018, 8, 1800734.
Ni_{SA}-MoS_2/CC	110	74	*Nano Energy*, 2018, **53**, 458.
MCM@MoS_2-Ni	161	81	*Adv. Funct. Mater.*, 2018, **28**, 1807086.
NPNi-MoS_2/rGO	205	71	*ACS Catal.*, 2018, **8**, 8107.
$Cu_{2-x}S$-MoS_2	320	60	*Chem. Mater.*, 2018, **30**, 4489.
$Mo_{0.5}W_{0.5}S_2$	138	55	*ACS Catal.*, 2018, **8**, 9529.
MoS_2(11.1% S vacancy)	520	155	*J. Am. Chem. Soc.*, 2018, **140**, 16773.
MoS_2-GNR	205	50	*Adv. Funct. Mater.*, 2018, **28**, 1802744.
MoS_2-MoP/C	136	58	*J. Mater. Chem. A*, 2018, **6**, 616.
Co-$^{S}MoS_2$	220	92	*Chem. Sci.*, 2018, **9**, 4769.
(1T/2H) MoS_2/α-MoO_3	232	81	*J. Mater. Chem. A*, 2018, **6**, 15320
MoS_2/rGO	154	77	*Chem. Commun.*, 2019, **55**, 2078.
MoS_2/MoP/NC	161	58	*J. Mater. Chem. A*, 2018, **6**, 24783.
MoS_2/CNT-2	194	53	*Nanoscale*, 2020, **12**, 1109.
MoS_2@CoS_2-20%	96	60	This work

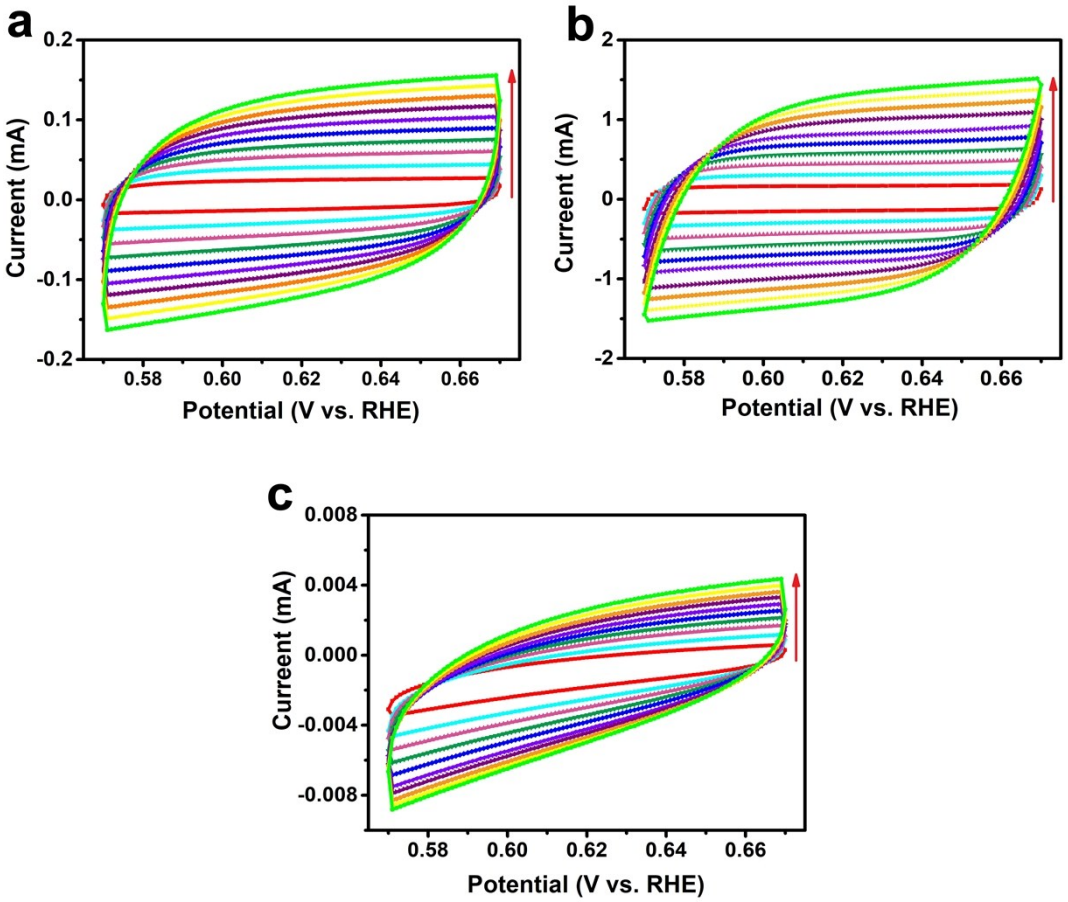

Fig. S6 CV curves of (a) MoS_2@CoS_2, (b) MoS_2, and (c) CoS_2 acquired at scan rates of 0.02, 0.04, 0.06, 0.08, 0.10, 0.12, 0.14, 0.16, 0.18, and 0.20 V s^{-1}.

The electrochemical active surface area (ECSA) is measured via a double layer capacitance (C_{dl}) method.[9, 10] In the non-Faradaic potential region, the measured current in CV is attributed to double-layer charging current (*i*), which is equal to the product of scan rate (*v*) and double layer capacitance (C_{dl}), as expressed by equation (1):

$$i = vC_{dl} \quad (1)$$

Thus, a plot of a series *i* as a function of *v* yields a straight line whose slope is C_{dl}. Once the C_{dl} is obtained, the ECSA can be calculated according to equation (2):

$$ECSA=C_{dl}/C_s \quad (2)$$

Where the C_s is the specific capacitance of planar surface. In this work, a typical C_s value of 0.040 mF cm^{-2} for MoS_2 material was adopted for the estimation of ECSA.[11]

The catalyst inks were prepared via the aforementioned procedures except the absence of carbon black. For the determination of C_{dl}, CV curves were measured in a potential range of 0.57~0.67 V at scan rates of 0.02, 0.04, 0.06, 0.08, 0.10, 0.12, 0.14, 0.16, 0.18, and 0.20 V s^{-2}. The CV curves of MoS_2@CoS_2, MoS_2 and CoS_2 recorded at various scan rates are shown in Fig. S6. The anodic currents (i_a) and cathodic currents (i_c) at 0.62 V were extracted for further analysis. C_{dl} was then obtained by plotting i, $0.5(i_a - i_c)$, as a function of scan rate, and the results were shown in Fig. 3c. The C_{dl} of MoS_2@CoS_2, MoS_2 and CoS_2 are determined to be 0.606, 6.383 and 0.015 mF, respectively. Accordingly, the ECSA is calculated to be 15.15 cm^2 for MoS_2@CoS_2, 159.58 cm^2 for MoS_2, and 0.38 cm^2 for CoS_2 when a C_s of 0.040 mF is considered.

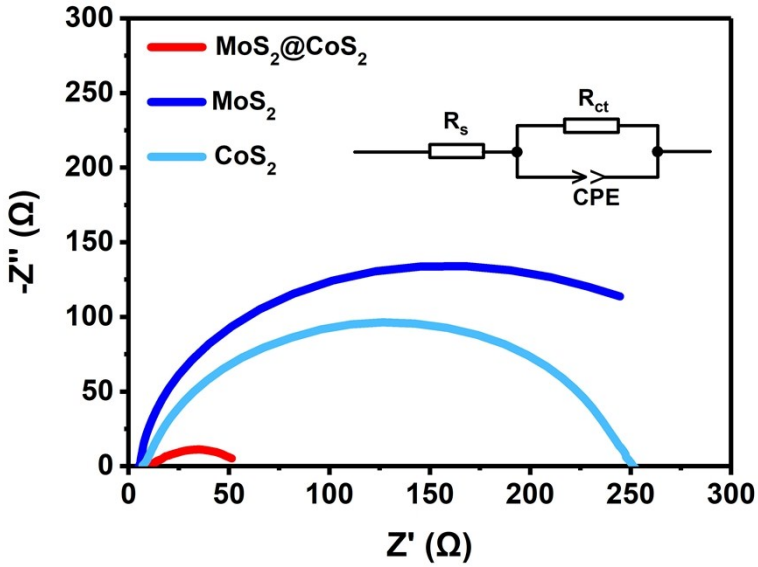

Fig. S7 Nyquist plots of MoS_2@CoS_2, MoS_2 and CoS_2 recorded at a static overpotential of 200 mV.

The impedance behaviors can be depicted with the equivalent circuit model as displayed in inset of Fig. S7. According to the fitted results, the electrochemical charge transfer resistance (R_{ct}) of MoS_2@CoS_2, MoS_2, and CoS_2 in HER are determined to be 46, 319, and 242 Ω, respectively. The series resistance of the electrochemical cell is determined to be 5.4 Ω according to the real component value of the impedance at the minimum of the Nyquist plot.[12]

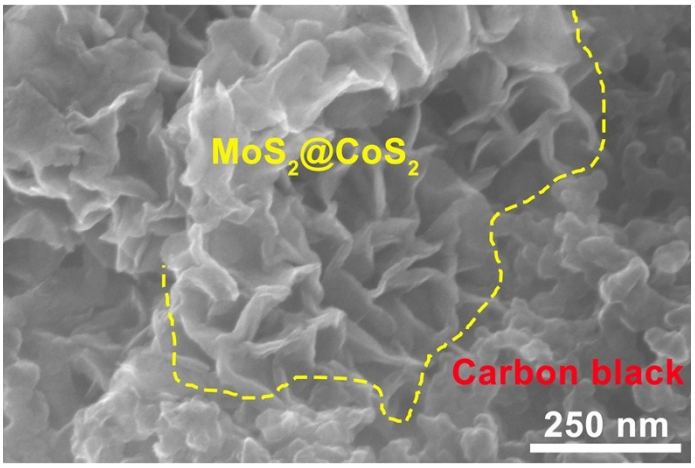

Fig. S8 SEM image of $MoS_2@CoS_2$ acquired after 1000 continuous CV cycles in a potential range of -0.15 ~ 0.1 V at a scan rate of 100 mV s^{-1}.

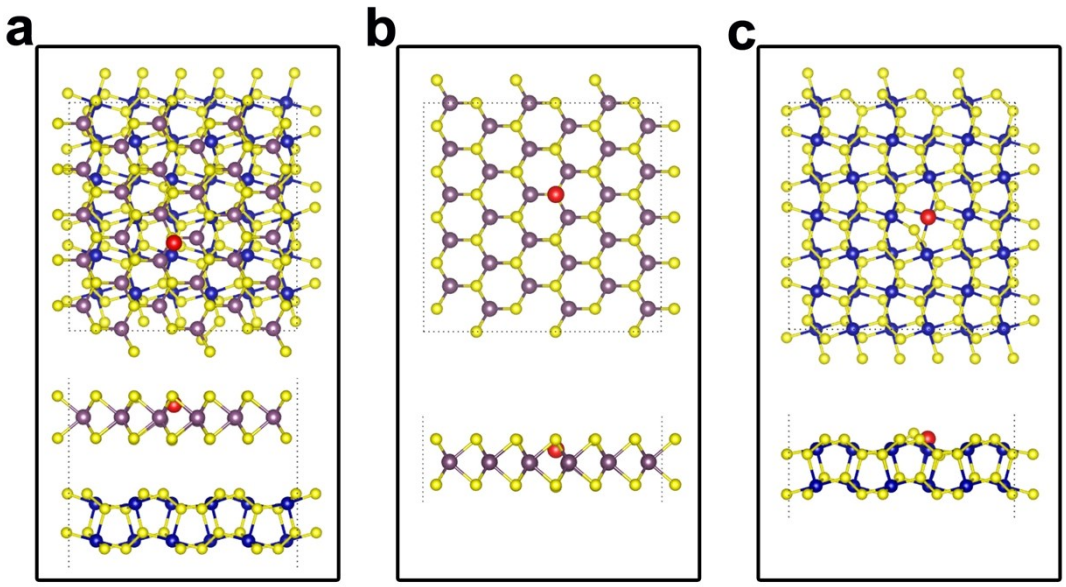

Fig. S9 Top and side views of hydrogen adsorption configurations of (a) MoS_2@CoS_2 heterojunction, (b) MoS_2 (S-vacancy), and (c) CoS_2 (001).

Reference:

1. J. Ekspong, R. Sandström, L. P. Rajukumar, M. Terrones, T. Wågberg and E. Gracia-Espino, *Adv. Funct. Mater.*, 2018, **28**, 1802744.
2. X. Wu, S. Zhou, Z. Wang, J. Liu, W. Pei, P. Yang, J. Zhao and J. Qiu, *Adv. Energy Mater.*, 2019, **9**, 1901333.
3. H. Zhang, L. Yu, T. Chen, W. Zhou and X. W. Lou, *Adv. Funct. Mater.*, 2018, **28**, 1807086.
4. G. Kresse and J. Furthmüller, *Comput. Mater. Sci.*, 1996, **6**, 15-50.
5. G. Kresse and J. Furthmüller, *Phys. Rev. B*, 1996, **54**, 11169-11186.
6. J. K. Nørskov, T. Bligaard, A. Logadottir, J. Kitchin, J. G. Chen, S. Pandelov and U. Stimming, *J. Electrochem. Soc.*, 2005, **152**, J23-J26.
7. X. Huang, Z. Zeng and H. Zhang, *Chem. Soc. Rev.*, 2013, **42**, 1934-1946.
8. B. Dutta, Y. Wu, J. Chen, J. Wang, J. He, M. Sharafeldin, P. Kerns, L. Jin, A. M. Dongare, J. Rusling and S. L. Suib, *ACS Catal.*, 2019, **9**, 456-465.
9. H. Wang, X. Xiao, S. Liu, C. L. Chiang, X. Kuai, C. K. Peng, Y. C. Lin, X. Meng, J. Zhao, J. Choi, Y. G. Lin, J. M. Lee and L. Gao, *J. Am. Chem. Soc.*, 2019, **141**, 18578-18584.
10. C. C. L. McCrory, S. Jung, J. C. Peters and T. F. Jaramillo, *J. Am. Chem. Soc.*, 2013, **135**, 16977-16987.
11. C. Wang, B. Tian, M. Wu and J. Wang, *ACS Appl. Mater. Interfaces*, 2017, **9**, 7084-7090.
12. X. Tan, J. Shen, N. Semagina and M. Secanell, *J. Catal.*, 2019, **371**, 57-70.